

Floquet engineering of long-range p-wave superconductivity

Mónica Benito, Álvaro Gómez-León, Victor Bastidas, Tobias Brandes, Gloria Platero

Angaben zur Veröffentlichung / Publication details:

Benito, Mónica, Álvaro Gómez-León, Victor Bastidas, Tobias Brandes, and Gloria Platero. 2014. "Floquet engineering of long-range p-wave superconductivity." *Physical Review B* 90: 205127. <https://doi.org/10.1103/PhysRevB.90.205127>.

Nutzungsbedingungen / Terms of use:

licgercopyright

Dieses Dokument wird unter folgenden Bedingungen zur Verfügung gestellt: / This document is made available under these conditions:

Deutsches Urheberrecht

Weitere Informationen finden Sie unter: / For more information see:

<https://www.uni-augsburg.de/de/organisation/bibliothek/publizieren-zitieren-archivieren/publiz/>



Floquet engineering of long-range p -wave superconductivity

M. Benito,^{1,*} A. Gómez-León,^{1,2,3} V. M. Bastidas,⁴ T. Brandes,⁴ and G. Platero¹

¹*Instituto de Ciencia de Materiales, CSIC, Cantoblanco, Madrid E-28049, Spain*

²*Department of Physics & Astronomy, University of British Columbia, Vancouver, BC, Canada V6T 1Z1*

³*Pacific Institute of Theoretical Physics, Vancouver, BC, Canada V6T 1Z1*

⁴*Institut für Theoretische Physik, Technische Universität Berlin, Hardenbergstrasse 36, 10623 Berlin, Germany*

(Received 1 September 2014; published 19 November 2014)

Floquet Majorana fermions appear as steady states at the boundary of time-periodic topological phases of matter. In this work, we theoretically study the main features of these exotic topological phases in the periodically driven one-dimensional Kitaev model. By controlling the ac fields, we can predict topological phase transitions that should give rise to signatures of Majorana states in experiments. Moreover, the knowledge of the time dependence of these Majorana states allows one to manipulate them. Our work contains a complete analysis of the monochromatic driving in different frequency regimes.

DOI: [10.1103/PhysRevB.90.205127](https://doi.org/10.1103/PhysRevB.90.205127)

PACS number(s): 03.65.Vf, 03.67.Lx, 75.10.Pq, 05.30.Rt

I. INTRODUCTION

In recent years, the phases of matter with topological origins have received intense attention in the field of solid-state physics [1–7]. In topological superconductors, these phases result in elementary excitations with non-Abelian statistics [8,9]. The bulk-boundary correspondence shows how differences between bulk topologies give rise to edge states localized at the boundaries [10].

Driven systems constitute a fruitful arena to study topological states of matter because they exhibit topological features that are richer than those of time-independent systems. Of particular interest are periodically driven systems, which have many close analogies with static systems [11–16]. Floquet eigenstates and quasienergies are similar to eigenstates and energies of static systems, but the periodicity of the quasienergy spectrum introduces new features unique to periodically driven systems [12,15,17–20]. In fact, the complete characterization of the topology of a time-periodic Hamiltonian requires the search for new topological invariants [12,21–23].

In this work, we propose an analytic approach to describe the topological phases of a driven chain of spinless fermions with p -wave superconductivity, i.e., the one-dimensional Kitaev model [8]. The end states emerging in driven topological superconductors are called Floquet Majorana fermions, because they are the analogous counterpart for Majorana fermions in static systems [8,24–30]. The characterization of these excitations allows one to design protocols for their manipulation, which is potentially relevant for braiding operations, which are essential for fault-tolerant quantum computation [31]. Furthermore, periodic driving opens a new avenue to detect these elusive particles [19,32].

In recent years, some works have addressed the effect of ac driving fields in topological superconductors. Most of them are restricted to the high-frequency regime. Those addressing lower frequencies are mainly focused on numerical treatments [17,31,33,34]. A more complete analysis was done in the cases of periodically kicked systems [35] and steplike periodic pulses [20], including the definition of new

topological invariants, while the harmonic driving is treated just numerically [35].

In contrast to previous works, in this paper we develop a complete analysis of monochromatic driving for different frequency regimes, which is more feasible in experiments. Our analytical treatment allows us to characterize different topological phases by means of effective Hamiltonians in rotated reference frames. Furthermore, we address different ways to drive the Kitaev chain, giving rise to a variety of topological quantum phase transitions (TQPTs), which could be experimentally tested.

The correspondence between the Kitaev chain and the one-dimensional transverse Ising model [36] is used mainly as a mathematical tool to simplify the analysis and to set a different framework to probe the phase transitions. In this sense, our results not only have relevance in the field of topological states of matter, but they also provide insight into quantum magnetism under nonequilibrium situations [37–40].

The simple characterization of the driven system for arbitrary frequencies by means of rotations of frame is the most important result of our work. This allows us to obtain the wave function of the Majorana end states in an easy way and to understand the role of the quasienergies in the TQPTs. Moreover, we show that the driving protocols allow one to manipulate the effective interactions between different neighbors, generating effective models that are difficult to implement in time-independent systems. Apart from this, we establish a connection between the effective interactions generated in the Kitaev model under the effect of driving and the magnetic interactions in the Ising model.

In Sec. II, we introduce the model and describe the main tools used in this paper. In particular, the behavior of Floquet states and the Magnus expansion under a rotation of the reference frame is studied in detail. In Sec. III, we analyze the case of an ac driven chemical potential. In this section, we present a thorough discussion of the methodology used to determine the TQPTs, based on effective Hamiltonians in different frames. In Secs. IV and V, we consider different driving protocols and discuss the emergence of exotic phases. In particular, we discuss the effective long-range interactions arising under the control of the tunneling amplitude.

*m.benito@csic.es

II. MODEL AND TOOLS

The system we analyze consists of a chain with $N \gg 1$ sites. Each site j can be either empty or occupied by a spinless fermion f_j . It consists in the driven version of the one-dimensional Kitaev model [8],

$$H(t) = \frac{\mu(t)}{2} \sum_{j=1}^N (2f_j^\dagger f_j - 1) - \frac{w(t)}{2} \sum_{j=1}^N (f_j^\dagger f_{j+1} + \text{H.c.}) - \frac{\Delta(t)}{2} \sum_{j=1}^N (f_j^\dagger f_{j+1}^\dagger + \text{H.c.}), \quad (1)$$

where $\mu(t)$ is the chemical potential, $w(t)$ is the tunneling, and $\Delta(t)$ is the BCS superconducting pairing between nearest neighbors in the presence of driving. In the case of periodic boundary conditions, $f_{N+1} = f_1$, we can use a discrete Fourier transformation to obtain the bulk Hamiltonian,

$$H_k(t) = \begin{pmatrix} \mu(t) - w(t) \cos k & -i\Delta(t) \sin k \\ i\Delta(t) \sin k & -\mu(t) + w(t) \cos k \end{pmatrix} = [\mu(t) - w(t) \cos k] \sigma_k^z + \Delta(t) \sin k \sigma_k^y, \quad (2)$$

where σ_k^λ for $\lambda \in \{x, y, z\}$ are the Pauli matrices in Nambu space. Correspondingly, we can write Eq. (1) as $H(t) = \sum_{k>0} \Psi_k^\dagger H_k(t) \Psi_k$, where $\Psi_k^\dagger = (f_k^\dagger, f_{-k}^\dagger)$ and f_k are fermionic operators in reciprocal space [41].

The undriven model, i.e., $\mu(t) = \mu_0$, $w(t) = w_0$, and $\Delta(t) = \Delta_0$, undergoes a TQPT [8]. Given that $\Delta_0 > 0$, the system exhibits a topologically nontrivial phase when $\mu_0 < w_0$ and a topologically trivial behavior as long as $\mu_0 > w_0$. The Hamiltonian has particle-hole and time-reversal symmetry [36,42], and therefore the different topological phases can be classified by means of the value of a bulk \mathbb{Z} topological invariant, which corresponds to the winding number

$$W = \frac{1}{2\pi} \int_{-\pi}^{\pi} d\varphi_k, \quad (3)$$

where $\tan \varphi_k = \Delta_0 \sin k (\mu_0 - w_0 \cos k)^{-1}$. The winding number is $W = 1$ in the nontrivial phase and $W = 0$ in the trivial one. A chain in the nontrivial phase with open boundary conditions exhibits Majorana modes localized at the ends [8].

The Hamiltonian of the driven XY model in an external transverse field

$$H(t) = -\frac{1}{2} \sum_{j=1}^N [\mu(t) \sigma_j^x - J_z(t) \sigma_j^z \sigma_{j+1}^z - J_y(t) \sigma_j^y \sigma_{j+1}^y] \quad (4)$$

can be mapped exactly onto the Kitaev Hamiltonian in Eq. (1) by means of a Jordan-Wigner transformation [41]. The time-dependent anisotropies are related to the tunneling and the superconducting gap as $J_z(t) = [w(t) + \Delta(t)]/2$ and $J_y(t) = [w(t) - \Delta(t)]/2$. In the time-independent case, there is a correspondence between the magnetic phases of the spin system and the topological phases of the fermion model, i.e., the paramagnetic phase is related to the trivial phase, and the ferromagnetic phase corresponds to the nontrivial phase [43]. Under monochromatic driving, new magnetic phases arise, corresponding to new topological phases in the fermionic system.

A. Floquet theory under rotation of the reference frame

We analyze the effect of a periodic time dependence of the Hamiltonian in Eq. (1). In this case, $H(t+T) = H(t)$ (with $T = 2\pi/\omega$ the period of the driving), therefore the Floquet theory is applicable [44–46]. By using the Floquet states $|\psi_v(t)\rangle = e^{-i\epsilon_v t} |\phi_v(t)\rangle$, the time-dependent Schrödinger equation becomes an eigenvalue equation for the Floquet modes $|\phi_v(t+T)\rangle = |\phi_v(t)\rangle$, referred to as the Floquet equation,

$$[H(t) - i\partial_t] |\phi_v(t)\rangle = \epsilon_v |\phi_v(t)\rangle. \quad (5)$$

The operator $\mathcal{H}(t) = H(t) - i\partial_t$ is the Floquet Hamiltonian, its eigenvalues are the quasienergies ϵ_v , and the eigenvectors $|\phi_v(t)\rangle$ are the Floquet modes. The index v corresponds to the band index. The quasienergies ϵ_v are not uniquely defined [44–46]. Therefore, we restrict them to the first Brillouin zone $-\omega/2 \leq \epsilon_v \leq \omega/2$.

To simplify the resolution of the Floquet equation, one should find an appropriate rotating frame in which a simple effective Hamiltonian can be defined, as we describe below. First of all, we will clarify the effect of a rotation of frame in the Floquet formalism. In the rotating frame, given by the unitary transformation $\mathcal{S}(t)$, the Floquet equation becomes $[\tilde{H}(t) - i\partial_t] |\tilde{\phi}_v(t)\rangle = \epsilon_v |\tilde{\phi}_v(t)\rangle$, where the Hamiltonian in the new frame is

$$\tilde{H}(t) = \mathcal{S}^\dagger(t) H(t) \mathcal{S}(t) - i\mathcal{S}^\dagger(t) \dot{\mathcal{S}}(t), \quad (6)$$

and $|\tilde{\phi}_v(t)\rangle = \mathcal{S}^\dagger(t) |\phi_v(t)\rangle$. As a consequence, the quasienergies do not change, but the periodicity of the Floquet modes does,

$$|\tilde{\phi}_v(t+T)\rangle = \mathcal{S}^\dagger(t+T) \mathcal{S}(t) |\tilde{\phi}_v(t)\rangle. \quad (7)$$

The one-period time-evolution operator makes a state evolve as $U(T,0) |\psi(0)\rangle = |\psi(T)\rangle$. Apart from Eq. (5), the quasienergies can also be obtained from the eigenvalue equation $U(T,0) |\phi_v(0)\rangle = e^{-i\epsilon_v T} |\phi_v(0)\rangle$. If we are working in a rotated frame, we can use Eq. (7) to obtain the eigenvalue equation for the one-period evolution operator

$$\tilde{U}(T,0) |\tilde{\phi}_v(0)\rangle = e^{-i\epsilon_v T} \mathcal{S}^\dagger(T) \mathcal{S}(0) |\tilde{\phi}_v(0)\rangle. \quad (8)$$

As a consequence of this, the relation between quasienergies ϵ_v and eigenvalues of $\tilde{U}(T,0)$ depends on the matrix \mathcal{S} . A common method to study time-dependent systems is to calculate the eigenvalues of the one-period evolution operator [44–46]. Equation (8) shows the relationship between these eigenvalues in an arbitrary reference frame (given by \mathcal{S}) and the quasienergies.

B. Magnus expansion for effective Hamiltonians

Once we are in the most suitable reference frame, we define a time-independent effective Hamiltonian \tilde{H}_{eff} such that

$$\tilde{U}(T,0) = \exp(-i\tilde{H}_{\text{eff}} T), \quad (9)$$

with $\tilde{H}(t)$ periodic in time. The Fourier decomposition $\tilde{H}(t) = \sum_p e^{ip\omega t} \tilde{H}_p$ allows us to write a power series expansion in $\frac{1}{\omega}$ for the time-independent Hamiltonian, referred to as the

Magnus expansion [47,48],

$$\begin{aligned} \tilde{H}^{\text{eff}} = & \tilde{H}_0 + \frac{1}{\omega}[\tilde{H}_0, \tilde{H}_1] - \frac{1}{\omega}[\tilde{H}_0, \tilde{H}_{-1}] \\ & - \frac{1}{\omega}[\tilde{H}_{-1}, \tilde{H}_1] + \dots \end{aligned} \quad (10)$$

with an infinite number of terms. This series is only useful if it converges with a finite number of terms. The convergence is given by the condition $\int_0^T \|\tilde{H}(t)\| dt < \pi$, where $\|\tilde{H}(t)\|$ is the Euclidean norm of the Hamiltonian, as is discussed in Refs. [47,48]. At this point, the choice of the frame of reference is relevant, since the Hamiltonian in different frames $\tilde{H}(t)$ has different convergence conditions.

The previous explanations are valid for general time-periodic Hamiltonians. In particular, the expansion Eq. (10) can be used for a Bogoliubov–de Gennes Hamiltonian in Nambu space. In this case, the transformation into the rotating frame factorizes as $S = \bigotimes_{k>0} S_k$. For a given k , we can use Eq. (6) to obtain the transformation of Hamiltonian Eq. (2) into the rotating frame $\tilde{H}_k(t) = S_k^\dagger H_k(t) S_k - i S_k^\dagger \dot{S}_k(t)$. Therefore, the convergence condition reads

$$\int_0^T \|\tilde{H}_k(t)\| dt < \pi. \quad (11)$$

In Nambu space, Eq. (8) implies the eigenvalue problem for the Floquet modes,

$$\tilde{U}_k(T, 0) |\tilde{\phi}_{v,k}(0)\rangle = e^{-i\epsilon_{v,k}T} S_k^\dagger(T) S_k(0) |\tilde{\phi}_{v,k}(0)\rangle, \quad (12)$$

where $\epsilon_{v,k}$ is the v th band quasienergy dispersion, $|\tilde{\phi}_v(0)\rangle = \bigotimes_{k>0} |\tilde{\phi}_{v,k}(0)\rangle$, and $\tilde{U}(T, 0) = \bigotimes_{k>0} \tilde{U}_k(T, 0)$.

III. DRIVING THE CHEMICAL POTENTIAL

We focus here on the study of the topological properties of the Kitaev model with a time-dependent chemical potential. Therefore, we assume $w(t) = w_0$, $\Delta(t) = \Delta_0$, and $\mu(t) = \mu_0 + \frac{\mu_1}{2} \cos \omega t$, where μ_0 is a constant term and $\frac{\mu_1}{2}$ is the amplitude of the driving.

As the Kitaev model is described by a Bogoliubov–de Gennes Hamiltonian, the solutions give the spectrum of excitations. Due to the particle-hole symmetry, these excitations come in pairs such that creating an excitation with energy E is equivalent to annihilating the excitation with energy $-E$. It means $\gamma_E^\dagger |GS\rangle = \gamma_{-E} |GS\rangle$, where $|GS\rangle$ is the vacuum of excitations fulfilling $\gamma_E |GS\rangle = 0 \ \forall \ E > 0$. Given this symmetry, a zero-energy excitation will fulfill the Majorana condition $\gamma_0 = \gamma_0^\dagger$. In the driven case, excitations come also in pairs $\gamma_\epsilon(t) = \gamma_{-\epsilon}^\dagger(t)$, where ϵ is the quasienergy. Due to the periodicity of the quasienergies, not only $\epsilon = 0$ but also $\epsilon = \pm \frac{\omega}{2}$ excitations fulfill the Majorana condition $\gamma_{0, \frac{\omega}{2}} = \gamma_{0, \frac{\omega}{2}}^\dagger$ [17]. Therefore, a complete phase diagram has to take into account possible closings of the quasienergy spectrum at quasienergies $\epsilon = \pm \frac{\omega}{2}$, as well as $\epsilon = 0$. Furthermore, both quasienergy gaps can support Majorana end states, and the topological phase is characterized by two \mathbb{Z} topological invariants ($\mathbb{Z} \times \mathbb{Z}$). In the following, we present a method based on reference frame transformations to find the topological phase diagram of the

Hamiltonian Eq. (1). Moreover, our method provides the wave function of the Majorana excitations.

A. Reference frame choice

Let us consider first the convergence of the Magnus expansion in the laboratory frame $\tilde{H}(t) = H(t)$. We calculate the first harmonics of the Hamiltonian Eq. (2):

$$\begin{aligned} H_{k,0} &= \frac{1}{T} \int_0^T dt' H_k(t') \\ &= (\mu_0 - w_0 \cos k) \sigma_k^z + \Delta_0 \sin k \sigma_k^y, \\ H_{k,\pm 1} &= \frac{1}{T} \int_0^T dt' H_k(t') e^{\mp i \omega t} \\ &= \frac{\mu_1}{4} \sigma_k^z. \end{aligned} \quad (13)$$

Regardless of the value of the quasimomentum k , the first term of the Magnus expansion $H_{k,0}$ is already a good approximation if the frequency is much larger than the bandwidth $\tau = \mu_0 + w_0$ and the driving amplitude μ_1 . We will show below that by means of a rotation of frame, the convergence regions can be increased.

We work with a whole family of rotating frames given by the transformations $S_{k,\alpha}^\dagger(t) = e^{i\theta_\alpha(t)\sigma_k^z}$ with $\theta_\alpha(t) = \frac{\alpha\omega}{2}t + \frac{\mu_1}{2\omega} \sin \omega t$ for $\alpha \in \{0, \pm 1, \pm 2, \dots\}$. For $\alpha = 0$, we obtain the transformation into the interaction picture. The Hamiltonians in the rotating frame are

$$\begin{aligned} \tilde{H}_k^\alpha(t) &= \left(\mu_0 - \frac{\alpha\omega}{2} - w_0 \cos k \right) \sigma_k^z - i \Delta_0 \sin k e^{2i\theta_\alpha(t)} \sigma_k^+ \\ &\quad + i \Delta_0 \sin k e^{-2i\theta_\alpha(t)} \sigma_k^-. \end{aligned} \quad (14)$$

Given that $S_{k,\alpha}^\dagger(T) S_{k,\alpha}(0) = e^{i\alpha\pi\sigma_k^z}$, Eq. (12) becomes

$$\tilde{U}_k^\alpha(T, 0) |\tilde{\phi}_{v,k}(0)\rangle = e^{-i\epsilon_{v,k}T} e^{i\alpha\pi\sigma_k^z} |\tilde{\phi}_{v,k}(0)\rangle. \quad (15)$$

This leads to the eigenvalue equation for the effective bulk Hamiltonian in Eq. (9),

$$\tilde{H}_k^{\text{eff},\alpha} |\tilde{\phi}_{v,k}(0)\rangle = \left(\epsilon_{v,k} - \frac{\alpha\omega}{2} \sigma_k^z \right) |\tilde{\phi}_{v,k}(0)\rangle, \quad (16)$$

which implies that the quasienergies and the eigenvalues of the effective Hamiltonian are related by a $\frac{\alpha\omega}{2}$ shift. Due to the periodicity of the quasienergies, this shift is relevant just in the case of odd values of α .

For a given α , the transformed Hamiltonian of Eq. (14) has different regions of convergence, determined by the condition in Eq. (11). The Fourier components $\tilde{H}_{k,p}^\alpha \equiv \frac{1}{T} \int_0^T dt' \tilde{H}_k^\alpha(t') e^{-ip\omega t}$ of $\tilde{H}_k^\alpha(t)$ are given by

$$\begin{aligned} \tilde{H}_{k,p}^\alpha &= \left(\mu_0 - \frac{\alpha\omega}{2} - w_0 \cos k \right) \delta_{p,0} \sigma_k^z \\ &\quad - i \Delta_0 \sin k \mathcal{J}_{p-\alpha} \left(\frac{\mu_1}{\omega} \right) \sigma_k^+ \\ &\quad + i \Delta_0 \sin k \mathcal{J}_{-p-\alpha} \left(\frac{\mu_1}{\omega} \right) \sigma_k^-, \end{aligned} \quad (17)$$

where $\mathcal{J}_n(x)$ is the n th – order Bessel function. We remark that the eigenvalues of the Hamiltonian in Eq. (14) do not depend on the amplitude μ_1 . Then, the convergence condition

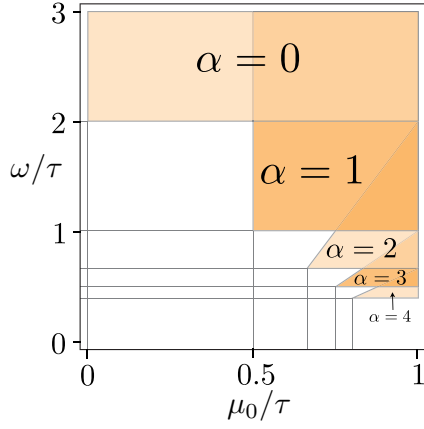


FIG. 1. (Color online) Regions of convergence of the Magnus expansion of $\tilde{H}_k^\alpha(t)$ for $\alpha \in \{0, 1, 2, 3, 4\}$ as a function of μ_0 and ω . To obtain a convergent Magnus expansion, the Hamiltonian $\tilde{H}_k^\alpha(t)$ has to fulfill the convergence condition Eq. (11) for all the values of k . At high frequency $\omega > 2\tau$, the series of $\tilde{H}_k^0(t)$ converges. For $\omega < 2\tau$, the successive $\tilde{H}_k^\alpha(t)$ have convergent series for some values of μ_0 . We consider a fixed bandwidth $\tau = \mu_0 + w_0$.

Eq. (11) is μ_1 -independent. Figure 1 depicts the regions of convergence of the Magnus expansion for successive $\tilde{H}_k^\alpha(t)$. The series of $\tilde{H}_k^0(t)$ converges in the high-frequency regime $\omega > 2\tau$. For $\omega < 2\tau$, the successive Hamiltonians $\tilde{H}_k^\alpha(t)$ have convergent series for different values of μ_0 .

By obtaining a frame where the Hamiltonian has a convergent Magnus series, we are able to get an approximation of the full quasienergy spectrum from the eigenvalues of the time-independent Hamiltonian of Eq. (10). Moreover, the effective Hamiltonian allows a simple description of the TQPTs. Within the regions of convergence, the effective Hamiltonian can be approximated by the zeroth-order term of Eq. (10). Thereby, we can use Eq. (17) with $p = 0$ as a zeroth-order effective Hamiltonian,

$$\tilde{H}_k^{\text{eff},\alpha} = (\mu_{\text{eff}} - w_0 \cos k) \sigma_k^z + \Delta_{\text{eff}} \sin k \sigma_k^y, \quad (18)$$

which is an effective Kitaev model with $\mu_{\text{eff}} = \mu_0 - \frac{\alpha\omega}{2}$ and $\Delta_{\text{eff}} = \Delta_0 \mathcal{J}_{-\alpha}(\frac{\mu_1}{\omega})$.

It is instructive to understand the form of the effective Hamiltonian in Eq. (18) in terms of Pauli matrices in real space. After a Jordan-Wigner and discrete Fourier transformation, we obtain an effective time-independent XY Hamiltonian [41],

$$\begin{aligned} \tilde{H}_k^{\text{eff},\alpha} = & -\frac{\mu_{\text{eff}}}{2} \sum_{j=1}^N \sigma_j^x - \frac{1}{4} (w_0 + \Delta_{\text{eff}}) \sum_{j=1}^N \sigma_j^z \sigma_{j+1}^z \\ & - \frac{1}{4} (w_0 - \Delta_{\text{eff}}) \sum_{j=1}^N \sigma_j^y \sigma_{j+1}^y. \end{aligned} \quad (19)$$

Apart from the existence of a paramagnetic phase, the effective anisotropies in Eq. (19) can be tuned to generate a ferromagnetic phase in the z direction (FMZ) or the y direction (FMY), as is discussed in Ref. [39]. In terms of Jordan-Wigner fermions in real space, the effective Hamiltonian Eq. (19)

reads

$$\begin{aligned} \tilde{H}_k^{\text{eff},\alpha} = & \frac{\mu_{\text{eff}}}{2} \sum_{j=1}^N (2f_j^\dagger f_j - 1) - \frac{w_0}{2} \sum_{j=1}^{N-1} (f_j^\dagger f_{j+1} + \text{H.c.}) \\ & - \frac{\Delta_{\text{eff}}}{2} \sum_{j=1}^{N-1} (f_j^\dagger f_{j+1}^\dagger + \text{H.c.}). \end{aligned} \quad (20)$$

The bulk topological invariant is the winding number, which for the effective Hamiltonian Eq. (18) becomes $W_\alpha = 1/2\pi \int_0^{2\pi} d\varphi_k^\alpha$, where $\tan \varphi_k^\alpha = \Delta_{\text{eff}} \sin k / (\mu_{\text{eff}} - w_0 \cos k)$. There is a trivial-nontrivial TQPT at $\mu_0 - \frac{\alpha\omega}{2} = w_0$, where the winding number changes from $W_\alpha = 0$ to $\neq 0$. In addition, in the nontrivial region, there are TQPTs between different topological phases at critical lines defined by $\mathcal{J}_{-\alpha}(\frac{\mu_1}{\omega}) = 0$. The different topological phases are classified by the winding number $W_\alpha = \text{sgn} \mathcal{J}_{-\alpha}(\frac{\mu_1}{\omega})$. Figure 2(a) depicts the phase diagram for $\alpha = 0$ and Fig. 2(b) depicts it for $\alpha = 1$.

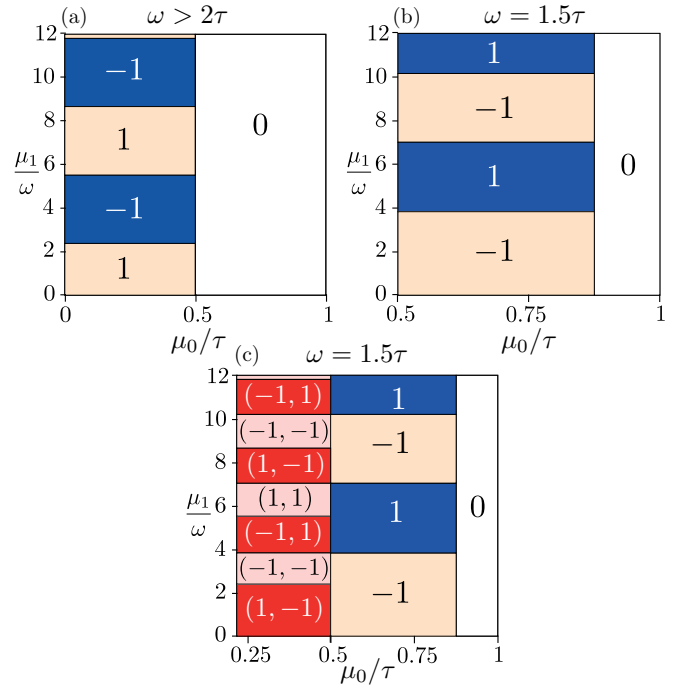


FIG. 2. (Color online) Phase diagram of the Kitaev Hamiltonian of Eq. (1) with time-dependent chemical potential $\mu(t) = \mu_0 + \frac{\mu_1}{2} \cos \omega t$. The white region is topologically trivial ($W = 0$), while the other ones are nontrivial ($W \neq 0$). (a) In the frequency regime $\omega > 2\tau$, $\tilde{H}_k^{\text{eff},0}$ is used to calculate the bulk invariant W_0 for all values of μ_0 , because the series of $\tilde{H}_k^0(t)$ converges. Transitions between the topological phases $W_0 = +1$ and -1 occur at zeros of $\mathcal{J}_0(\frac{\mu_1}{\omega})$. (b) For $\omega = 1.5\tau$, the series of $\tilde{H}_k^1(t)$ converges for $\mu_0 > 0.5\tau$. The trivial phase appears for $\mu_0 > 0.875\tau$ and transitions between phases $W_1 = 1$ and -1 take place at zeros of $\mathcal{J}_1(\frac{\mu_1}{\omega})$. (c) Depicts the extension of the phase diagram shown in (b) for $\omega = 1.5\tau$ to smaller values of μ_0 . Besides the phases $W_1 = 0, \pm 1$, we find new topological phases that are described by two topological invariants (W_0, W_1) , corresponding to the effective Hamiltonians $\tilde{H}_k^{\text{eff},0}$ and $\tilde{H}_k^{\text{eff},1}$. We consider a fixed bandwidth $\tau = \mu_0 + w_0$.

The family of effective Hamiltonians given by Eq. (18) can close only at zero quasienergy, while the quasienergies present also closings at $\epsilon = \frac{\omega}{2}$. The shift of Eq. (16) implies that a Hamiltonian with even α will describe closings of the gap at $\epsilon = 0$ and a Hamiltonian with odd α closings of the gap at $\epsilon = \pm \frac{\omega}{2}$. By now, we have found regions of the parameter space that can be described with only one effective Hamiltonian $\tilde{H}_k^{\text{eff},\alpha}$ for every k . Consequently, in these regions only one of the gaps ($\epsilon = 0$ or $\frac{\omega}{2}$) can close. However, it is possible to use two effective Hamiltonians at the same time, e.g., $\tilde{H}_k^{\text{eff},\alpha}$ and $\tilde{H}_k^{\text{eff},\alpha+1}$, to get a full convergence of the Magnus series in such a way that one of the Hamiltonians reproduces the 0 gap and the other one reproduces the $\frac{\omega}{2}$ gap. In the following, we probe that this is possible and show where it can be used and how it works.

B. Combination of frames

Looking at the convergence of the Magnus expansion, we realize that even when the series of $\tilde{H}_k^\alpha(t)$ does not converge for all k values, it is possible that it converges for some k values while $\tilde{H}_k^{\alpha+1}(t)$ converges for the rest. In that case, a complete convergence is possible using both. This concept increases the size of the regions that can be studied analytically in a good approximation.

This motivates the use of two effective Hamiltonians to classify the topological features of the system. Therefore, we use two invariants W_α and $W_{\alpha+1}$, which give a complete topological description encoded in the pair $(W_\alpha, W_{\alpha+1})$. In these cases, there are TQPTs at zeros of both $\mathcal{J}_\alpha(\frac{\mu_1}{\omega})$ and $\mathcal{J}_{\alpha+1}(\frac{\mu_1}{\omega})$. An example of this situation is shown in Fig. 2(c) for $\omega = 1.5\tau$, in which we extend the phase diagram of Fig. 2(b) to smaller values of μ_0 . Figure 1 shows that for $\omega > 2\tau$ the Magnus series of $\tilde{H}_k^0(t)$ converges independently of k and μ_0 . However, for values of k in a neighborhood of $k = 0$, the Magnus series converges even for a lower driving frequency $\omega = 1.5\tau$. This allows us to extend the phase diagram of Fig. 2(b), because the series of $\tilde{H}_k^1(t)$ also converges for values in the neighborhood of $k = \pi$ in the region $0.25\tau < \mu_0 < 0.5\tau$. In Appendix A, we discuss the features of the phase diagrams of Fig. 2 and compare them with the numerical result, obtaining a good agreement. Moreover, all the critical lines of the TQPTs are explained in detail from an analytic approach.

C. Majorana end states

The bulk-boundary correspondence involves the existence of end states localized at the boundary between different bulk topologies. In this section, we find the time evolution of the Majorana end state at the boundary between a nontrivial topological phase and the vacuum.

Let us assume that one of the effective Hamiltonians Eq. (18) converges in a particular region of the parameter space, as is depicted in Fig. 1. In the case of open boundary conditions, we can use the Majorana operators $a_{2j-1} = f_j + f_j^\dagger$ and $a_{2j} = -i(f_j - f_j^\dagger)$ as defined in Ref. [8] to write the

effective Hamiltonian Eq. (20) as follows:

$$\begin{aligned} \tilde{H}_k^{\text{eff},\alpha} = & \frac{\mu_{\text{eff}}}{2} \sum_{j=1}^N (ia_{2j}a_{2j-1} - 1) \\ & - \frac{i(w_0 + \Delta_{\text{eff}})}{4} \sum_{j=1}^{N-1} a_{2j}a_{2j+1} \\ & - \frac{i(-w_0 + \Delta_{\text{eff}})}{4} \sum_{j=1}^{N-1} a_{2j-1}a_{2j+2}. \end{aligned} \quad (21)$$

In the limit $\mu_{\text{eff}} \gg |w_0 + \Delta_{\text{eff}}|, |-w_0 + \Delta_{\text{eff}}|$ there are no zero-energy excitations. In the case $\mu_{\text{eff}} \ll |w_0 - \Delta_{\text{eff}}|$ and $\Delta_{\text{eff}} \simeq -w_0$ the third term dominates and the zero-energy excitations a_2 and a_{2N-1} with bulk invariant $W_\alpha = -1$ do not appear in the Hamiltonian, but they define the nonlocal fermion $\tilde{f} = \frac{1}{2}(a_2 + ia_{2N-1})$, which is topologically protected [8,9]. In the case of a semi-infinite chain with a large number of sites $N \gg 1$, we can obtain time evolution of the left end state in the laboratory frame,

$$\tilde{\gamma}(t) \approx -i(f_1 e^{-i\theta_\alpha(t)} - f_1^\dagger e^{i\theta_\alpha(t)}). \quad (22)$$

In the case in which $\mu_{\text{eff}} \ll |w_0 + \Delta_{\text{eff}}|$ and $\Delta_{\text{eff}} \simeq w_0$, the second term dominates and the Majorana operators a_1 and a_{2N} do not appear in the Hamiltonian [8]. Similarly to the previous case, they are combined into a nonlocal fermion $f = \frac{1}{2}(a_1 + ia_{2N})$. In this regime, the system possesses the bulk invariant $W_\alpha = 1$, and the time evolution of the mode localized at the first site reads

$$\gamma(t) \approx f_1 e^{-i\theta_\alpha(t)} + f_1^\dagger e^{i\theta_\alpha(t)}. \quad (23)$$

Interestingly, at discrete times $t = nT$, the edge states of Eqs. (22) and (23) are given by $\tilde{\gamma}(nT) \approx -(-1)^{n\alpha}i(f_1 - f_1^\dagger)$ and $\gamma(nT) \approx (-1)^{n\alpha}(f_1 + f_1^\dagger)$, respectively.

For a finite chain with N sites, the numerical calculation explained in Appendix B allows us to obtain the Floquet Majorana modes

$$\Psi_l(t) = \sum_{i=1}^N [u_{li}(t)f_i + v_{li}(t)f_i^\dagger]. \quad (24)$$

To compare our analytical results with numerical calculations, we consider Eqs. (22) and (23) for $\alpha = 1$. In this case, the quasienergy gap closes at $\epsilon = \pm\omega/2$. Therefore, to obtain the edge states for a chain with $N = 60$ sites, we numerically calculate the coefficients $u_i(t)$ and $v_i(t)$ for a state with quasienergy $\epsilon = \pm\omega/2$, as we explain in Appendix B. By assuming a fixed bandwidth $\tau = \mu_0 + w_0$, we perform the calculation for the parameters $\omega = 1.5\tau$ and $\mu_0 = 0.75\tau$.

To verify that Eq. (22) gives us the correct stroboscopic dynamics for $\tilde{\gamma}(nT)$, we plot the imaginary part of the coefficients $u_i(t)$ and $v_i(t)$ in Fig. 3(a). One can see that at discrete times $t = nT$ they are approximately in agreement with our analytical results. In addition, Fig. 3(b) depicts the real part of $u_i(t)$ and $v_i(t)$ at discrete times and shows qualitative agreement with the stroboscopic evolution $\gamma(nT)$ obtained from Eq. (23). The states spread along the vicinity of the end, because the solution of Eqs. (22) and (23) is only exact in the

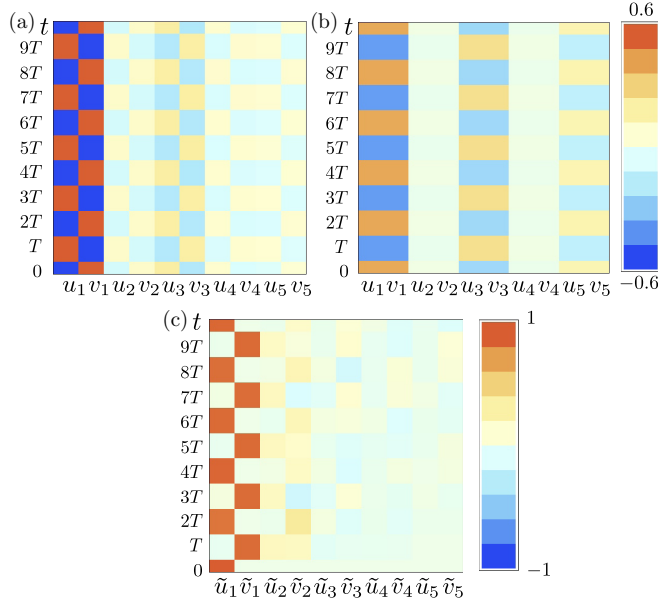


FIG. 3. (Color online) (a,b) Temporal stroboscopic evolution of the stationary left end state for a finite chain with $N = 60$ sites. The color indicates the value of coefficients u_i and v_i in Eq. (24) (i corresponding to the left Majorana end mode) for the first five sites. For a frequency $\omega = 1.5\tau$, we have performed numerical calculations in the case of a driven chemical potential $\mu(t) = \mu_0 + \frac{\mu_1}{2} \cos \omega t$ with $\mu_0 = 0.75\tau$. (a) Depicts the evolution for $\frac{\mu_1}{\omega} = 1$, being $\mathcal{J}_{-1}(\frac{\mu_1}{\omega}) < 0$, and (b) for $\frac{\mu_1}{\omega} = 4.5$, when $\mathcal{J}_{-1}(\frac{\mu_1}{\omega}) > 0$. The stroboscopic dynamic agrees with the predicted one. (c) Shows the evolution of coefficients \tilde{u}_i and \tilde{v}_i [Eq. (26)] in case $\mu_0 = 0.3\tau$ and $\frac{\mu_1}{\omega} = 1$ imposing the initial condition $\Gamma(0) = f_1$ at $t = 0$. The predicted double period electron-hole oscillations are observed. We consider a fixed bandwidth $\tau = \mu_0 + w_0$.

limit $w_0 = \Delta_0 \mathcal{J}_{-1}(\frac{g_1}{\omega}) \gg \mu_0 - \frac{\omega}{2}$, but the weight of the states along the chain decreases exponentially.

In a case with end states in the gaps $\epsilon = 0$ and $\epsilon = \omega/2$, we require the use of the effective Hamiltonians $\tilde{H}_k^{\text{eff},\alpha}$ and $\tilde{H}_k^{\text{eff},\alpha+1}$. For instance, in the phase with the invariant $(W_0, W_1) = (1, -1)$, there are two Majorana end states, one in each gap,

$$\begin{aligned} \gamma_{\epsilon=0}(t) &\approx f_1 e^{-i\theta_0(t)} + f_1^\dagger e^{i\theta_0(t)}, \\ \gamma_{\epsilon=\frac{\omega}{2}}(t) &\approx -i(f_1 e^{-i\theta_1(t)} - f_1^\dagger e^{i\theta_1(t)}), \end{aligned} \quad (25)$$

for parameters $\omega = 1.5\tau$, $\mu_0 = 0.3\tau$, and $\mu_1/\omega = 1$. The fact that two nondegenerate (in quasienergy) end states are present in the system generates interferences characteristic of ac-driven topological systems [17,18]. To see the interference of states in both gaps, we are interested in the study of the time evolution of the system for a given initial condition. According to the approximated Majorana modes, if the initial excitation is $\Gamma(0) = f_1$, it can be written as $\Gamma(0) \approx [\gamma_{\epsilon=0}(0) + i\gamma_{\epsilon=\frac{\omega}{2}}(0)]/2$. Therefore, the evolved excitation is known to be $\Gamma(t) \approx [\gamma_{\epsilon=0}(t) + i\gamma_{\epsilon=\frac{\omega}{2}}(t)]/2$ at all times. At discrete times $t = nT$ the system exhibits a doubly periodic stroboscopic dynamics $\Gamma(nT) \approx \frac{f_1}{2} [1 + (-1)^n] + \frac{f_1^\dagger}{2} [1 - (-1)^n]$. In Appendix B, we explain how to obtain the evolved excitation

after an imposed initial condition, written as

$$\Gamma(t) = \sum_{i=1}^N [\tilde{u}_i(t) f_i + \tilde{v}_i(t) f_i^\dagger]. \quad (26)$$

We show the predicted doubly periodic oscillations in Fig. 3(c), where we plot the real part of the numerically obtained coefficients $\tilde{u}_i(t)$ and $\tilde{v}_i(t)$ of $\Gamma(t)$ in Eq. (26) at discrete times, for the initial condition $\Gamma(0) = f_1$. These oscillations are due to the interference of states in both gaps.

IV. DRIVING THE TUNNELING AND BCS PAIRING

In this section, we apply the findings of the preceding section to study the Kitaev model considering a different driving protocol, which introduces different phases with more end states. We consider the Kitaev chain of spinless fermions f_j given in Eq. (1) with a constant chemical potential μ_0 and time-periodic tunneling and BCS pairing such that $w(t) = \Delta(t) = J(t) = J_0 + \frac{J_1}{2} \cos \omega t$. Using the equivalence of the Kitaev and Ising models and a duality transformation, the resolution of the problem is straightforward.

After a Jordan-Wigner transformation, this model corresponds to the one-dimensional Ising model in an external magnetic field,

$$H(t) = -\frac{\mu_0}{2} \sum_{j=1}^N \sigma_j^x - \frac{J(t)}{2} \sum_{j=1}^N \sigma_j^z \sigma_{j+1}^z, \quad (27)$$

which follows directly from the Hamiltonian Eq. (4) with $\mu(t) = \mu_0$, $J_z(t) = J(t)$, and $J_y(t) = 0$. Under the duality transformation $\sigma_j^x = \mu_j^z \mu_{j+1}^z$, $\sigma_j^z = \prod_{k \leq j} \mu_k^x$ [43], we get what is called the dual Hamiltonian of Eq. (27),

$$H^{(D)}(t) = -\frac{J(t)}{2} \sum_{j=1}^N \mu_j^x - \frac{\mu_0}{2} \sum_{j=1}^N \mu_j^z \mu_{j+1}^z, \quad (28)$$

which is exactly the corresponding Ising model to the system studied in the preceding section with $\mu(t) \rightarrow J(t)$ and $\Delta(t) = w(t) \rightarrow \mu_0$ in Eq. (4)—in this case, however, written in terms of the Pauli matrices μ_i^λ . This means that the quasienergy spectrum is the same, and by performing the inverse duality transformation to the effective Hamiltonians in Eq. (19), we obtain the effective Hamiltonians for the new driven system Eq. (27). The effective spin model reads

$$\begin{aligned} \tilde{H}_\alpha^{\text{eff}} &= -\frac{J_{\text{eff}}}{2} \sum_{j=1}^N \sigma_j^z \sigma_{j+1}^z - \frac{\mu_0}{4} \left[1 + \mathcal{J}_{-\alpha} \left(\frac{J_1}{\omega} \right) \right] \sum_{j=1}^N \sigma_j^x \\ &\quad + \frac{\mu_0}{4} \left[1 - \mathcal{J}_{-\alpha} \left(\frac{J_1}{\omega} \right) \right] \sum_{j=1}^N \sigma_{j-1}^z \sigma_j^x \sigma_{j+1}^z, \end{aligned} \quad (29)$$

where $J_{\text{eff}} = J_0 - \frac{\alpha\omega}{2}$. The last term is a three-spins interaction, which in the spinless fermion basis is a second-neighbor interaction term that will give rise to a new topological phase with winding number $W_\alpha = 2$.

The phase diagrams for the present configuration are like the ones found in the previous section (Fig. 2), but with a different value of the topological invariants. The phase diagram in the high-frequency regime is shown in Fig. 4(a). It is important to

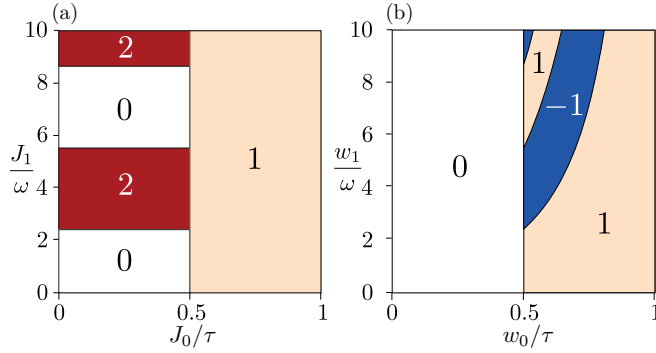


FIG. 4. (Color online) Phase diagram for $\omega > 2\tau$ in the case of $\mu(t) = \mu_0$, (a) $\Delta(t) = w(t) = J(t) = J_0 + \frac{J_1}{2} \cos \omega t$, (b) $w(t) = w_0 + \frac{w_1}{2} \cos \omega t$, and $\Delta(t) = \Delta_0$. The white region is topologically trivial ($W = 0$), the light-orange ($W = 1$) and blue ($W = -1$) regions are nontrivial phases with one end state, and the brown region ($W = 2$) is a nontrivial phase with two end states.

notice that the trivial region in the static case ($J_1 = 0$) becomes nontrivial in the high-frequency regime. In Fig. 4(a), the bulk invariant can be tuned from trivial ($W_\alpha = 0$) to nontrivial ($W_\alpha = 2$), depending on the strength of the driving. In contrast to this, in the case of a driven chemical potential, the trivial region remains trivial at high frequency independently of the strength of the driving.

In the case $J_{\text{eff}} > \mu_0$, the chain supports end states given in Eq. (23), while no end states are present if $J_{\text{eff}} < \mu_0$ and $\mathcal{J}_{-\alpha}(\frac{J_1}{\omega}) > 0$. To study the existence of end states in the new phase [$J_{\text{eff}} < \mu_0$ and $\mathcal{J}_{-\alpha}(\frac{J_1}{\omega}) < 0$], we write the second-neighbor interaction term in terms of Majorana operators [8] $a_{2j-1} = f_j + f_j^\dagger$ and $a_{2j} = -i(f_j - f_j^\dagger)$ as $H \propto i \sum_j a_{2j-2} a_{2j+1}$. Therefore, if the chain is semi-infinite, the Majorana operators a_1 and a_3 will not appear in the Hamiltonian, being therefore two Majorana end states:

$$\begin{aligned} \gamma_a(t) &\simeq f_1 e^{-i\theta_a(t)} + f_1^\dagger e^{i\theta_a(t)}, \\ \gamma_b(t) &\simeq f_3 e^{-i\theta_a(t)} + f_3^\dagger e^{i\theta_a(t)}. \end{aligned} \quad (30)$$

To sum up, we have found an effective Kitaev model with second-neighbor tunneling and BCS pairing and, consequently, a topological phase hosting two Majorana end states.

V. DRIVING THE TUNNELING

Finally, and for completeness, we are interested in the consequences of a driving just of the tunneling term of the Kitaev model Eq. (1). We consider a constant chemical potential μ_0 , BCS pairing Δ_0 , and a monochromatic driving of the tunneling strength $w(t) = w_0 + \frac{w_1}{2} \cos \omega t$.

In this section, we obtain a solution in the high-frequency limit by means of a transformation into the interaction picture $\mathcal{S}_k = e^{i\theta(t) \cos k \sigma_k^z}$, where $\theta(t) = \frac{w_1}{2\omega} \sin \omega t$. The high-frequency effective Hamiltonian is

$$\tilde{H}_k^{\text{eff}} = (\mu_0 - w_0 \cos k) \sigma_k^z + \Delta_0 \sin k \mathcal{J}_0\left(\frac{w_1}{\omega} \cos k\right) \sigma_k^y. \quad (31)$$

The transition between trivial and nontrivial phases takes place at $\mu_0 = w_0$. More gap closings are found when $\mathcal{J}_0(\frac{w_1}{\omega} \cos k) = 0$ and $\mu_0 - w_0 \cos k = 0$. This implies $\mathcal{J}_0(\frac{w_1}{\omega} \frac{\mu}{w_0}) = 0$, as long as $\mu_0 < w_0$. The high-frequency phase diagram is shown in Fig. 4(b).

Despite its apparent simplicity, the Bogoliubov Hamiltonian Eq. (31) contains a rich physical meaning. The first term of Eq. (31) is trivial in the sense that it describes the local term proportional to the chemical potential μ_0 and the tunneling between nearest neighbors with amplitude w_0 . The second term, however, generates new features of the BCS pairing, which arise from effective long-range interactions in real space. To understand the nature of these interactions arising in Eq. (31), let us consider the BCS term

$$V = \frac{\Delta_0}{2i} \sum_k \sin k \mathcal{J}_0\left(\frac{w_1}{\omega} \cos k\right) (f_{-k} f_k - f_k^\dagger f_{-k}^\dagger). \quad (32)$$

Performing the inverse Fourier transformation in order to obtain the real-space representation is not straightforward due to the k dependence in the argument of the Bessel function. However, we can use the expansion of the Bessel function in power series of its argument,

$$\begin{aligned} \mathcal{J}_0(z_k) &= \sum_{m=0}^{\infty} \frac{(-1)^m}{m!^2} \left(\frac{w_1}{2\omega} \cos k\right)^{2m} \\ &= \sum_{m=0}^{\infty} \sum_{r=0}^{2m} \frac{(-1)^m}{m!^2} \left(\frac{w_1}{4\omega}\right)^{2m} \binom{2m}{r} e^{2i(m-r)k}, \end{aligned} \quad (33)$$

where the binomial theorem was used. After some manipulations, we get

$$V = -\frac{\Delta_0}{2} \sum_{j=1}^N \sum_{m=0}^{\infty} \sum_{r=0}^{2m} C_{m,r} (f_j^\dagger f_{j+a_{m,r}}^\dagger - f_j^\dagger f_{j+b_{m,r}}^\dagger + \text{H.c.}), \quad (34)$$

with coefficients

$$C_{m,r} = \frac{(-1)^m}{2(m!)^2} \left(\frac{w_1}{4\omega}\right)^{2m} \binom{2m}{r}. \quad (35)$$

This means that V is an effective BCS interaction term with a neighbors range given by

$$\begin{aligned} a_{m,r} &= 2(m-r) + 1, \\ b_{m,r} &= 2(m-r) - 1. \end{aligned} \quad (36)$$

Finally, the Hamiltonian in real space can be simplified to

$$\begin{aligned} \tilde{H}^{\text{eff}} &= \frac{\mu_0}{2} \sum_{j=1}^N (2f_j^\dagger f_j - 1) - \frac{w_0}{2} \sum_{j=1}^N (f_j^\dagger f_{j+1} + \text{H.c.}) \\ &\quad - \frac{\Delta_0}{2} \sum_{j=1}^N \sum_{l=1,3,\dots}^N g_l(w_1) (f_j^\dagger f_{j+l}^\dagger + \text{H.c.}), \end{aligned} \quad (37)$$

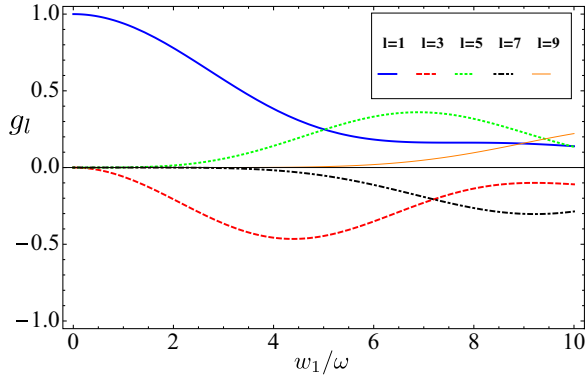


FIG. 5. (Color online) BCS interaction strength g_l as a function of w_1/ω for neighbors $l = 1, 3, 5, 7, 9$. Notice that the sign of the interaction is $(-1)^{\frac{l-1}{2}}$.

where the strength of the BCS interaction between l th neighbors is given by the function $g_l(w_1)$:

$$g_l(w_1) = 2 \left[D \left(\frac{l-1}{2} \right) - D \left(\frac{l+1}{2} \right) \right],$$

$$D(d) = \sum_{m=0}^{\infty} C_{m,m-d}. \quad (38)$$

We show the function $g_l(w_1)$ in Fig. 5. As expected, for small w_1 the first-neighbor interaction is larger. However, as the amplitude of the driving increases, the next-neighbor interactions become important. Since the sign between the first-neighbor and third-neighbor interaction is opposite (Fig. 5), the winding number changes sign, as was shown in Fig. 4(b).

In the reciprocal space, the Hamiltonian Eq. (37) reads

$$\tilde{H}_k^{\text{eff}} = (\mu_0 - w_0 \cos k) \sigma_k^z + \Delta_0 \sum_{l=1,3,\dots}^N g_l(w_1) \sin kl \sigma_k^y, \quad (39)$$

which shows how the driving allows us to engineer exotic phases of matter. Finally, we derive the expression of the long-range BCS interaction arising in Eq. (37) in terms of Pauli matrices in real space. This allows us to obtain the effective spin model,

$$\tilde{H}^{\text{eff}} = -\frac{\mu_0}{2} \sum_{j=1}^N \sigma_j^x - \frac{w_0}{4} \sum_{j=1}^N (\sigma_j^z \sigma_{j+1}^z + \sigma_j^y \sigma_{j+1}^y)$$

$$- \frac{\Delta_0}{4} \sum_{j=1}^N \sum_{l=1,3,\dots}^N g_l(w_1) (\sigma_j^z M_{j,l}^x \sigma_{j+l}^z - \sigma_j^y M_{j,l}^x \sigma_{j+l}^y), \quad (40)$$

where $M_{i,l}^x = \sigma_{i+1}^x \cdots \sigma_{i+l-1}^x$. Long-range spin interactions are generated by means of the ac driving of the tunneling, which in the spin basis corresponds to a time-periodic anisotropy between the Z and Y directions [see Eq. (4)].

The Kitaev chain is a simple model that considers spinless fermions. A physical realization of this model is a one-dimensional wire with Rashba spin-orbit interaction, Zeeman splitting, and proximity-induced s -wave superconductivity [29]. In this realization, the periodic variation of the

chemical potential in the wire is possible by means of an alternating gate voltage applied to the substrate, as suggested in [33]. Another proposed realization of the Kitaev chain consists in using semiconductor quantum dots coupled to superconducting grains [49]. In this setup, the access to the other parameters is more suitable because the relations between the experimental and effective parameters are more simple [50]. The advantage of our analytical approach is that it allows us to easily predict the TQPTs at any frequency regime, i.e., not only in the high-frequency regime but also at intermediate and low frequencies. Our approach allows for a comparison with future experiments performed in a full range of frequency regimes of the external driving, as long as we restrict ourselves to the studied convergence regions.

VI. CONCLUSIONS

We have discussed the nonequilibrium TQPTs in the Kitaev model with three different driving protocols. In all the cases, we focus on the effect of monochromatic control of the parameters, which is a realistic driving. By means of rotations of frame, we get a completely analytical description of the topological phase diagram in a wide range of frequencies for some values of the parameters. Moreover, we are able to provide an approximated wave function of the Majorana end states.

The equivalence between the Kitaev model and the Ising model allows us to use a simple duality transformation to relate the previous results with the resolution of a Kitaev chain whose tunneling and BCS parameters are varied in time harmonically. In this case, new features are found, such as the appearance of two Majorana end states at high frequency.

Finally, by only driving the tunneling, very interesting effective models with long-range superconductivity arise. Our analysis addressing three different ways of driving with harmonic time-dependent potentials gives a full picture of the consequences of the topological phases at arbitrary frequencies. It allows us to design the most efficient way to search signatures of Floquet Majorana fermions by appropriated drive of the system. Moreover, we briefly explain the equivalence of these properties in the spin chain basis, emphasizing the novelties detected.

ACKNOWLEDGMENTS

M.B., A.G.-L., and G.P. acknowledge the Spanish Ministry of Economy and Competitiveness through Grant No. MAT2011-24331 and the associated FPI scholarship (M.B.). V.M.B. and T.B. wish to acknowledge financial support by the Deutsche Forschungsgemeinschaft (DFG) via GRK 1558, Grants No. BRA 1528/7, No. BRA 1528/8, and No. SFB 910.

APPENDIX A: EXPLICIT DESCRIPTION OF THE COMBINATION OF FRAMES

In this Appendix, we discuss the phase diagram of Fig. 2 for $\omega = 1.5\tau$. We analyze in more detail the origin of each TQPT and calculate the critical lines numerically in order to check the validity of our approximated method used in Sec. III. In Fig. 6(a), the critical lines corresponding to the 0

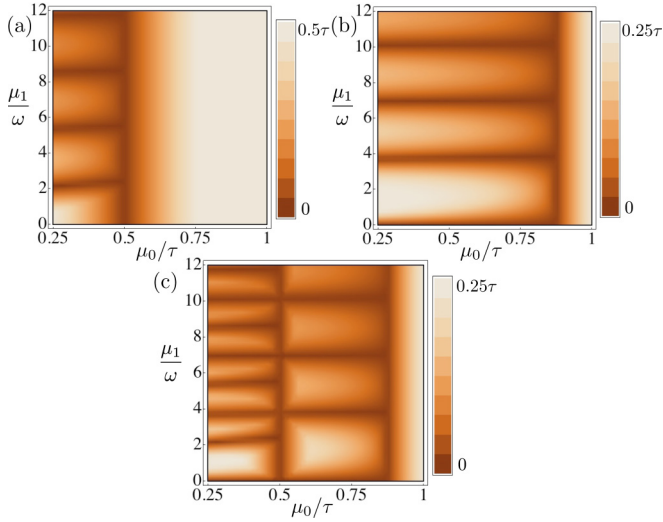


FIG. 6. (Color online) Phase diagram for $\omega = 1.5\tau$ in the case of a driven chemical potential. The dark lines show the closings of (a) the 0 gap, (b) the $\frac{\omega}{2}$ gap, and (c) both gaps. The whole topological phase diagram is given by (c), which agrees perfectly with the analytical result in Fig. 2.

gap of quasienergies are shown, while the critical lines of the $\frac{\omega}{2}$ gap are represented in Fig. 6(b). The dark lines indicate the occurrence of TQPTs. The combination of both gaps provides the whole topological phase diagram depicted in Fig. 6(c).

By means of the method developed in the main text, we are able to explain the different phases present in this phase diagram. In the regime $\tau < \omega < 2\tau$ and for any value of k , the convergence condition of Eq. (11) for $\tilde{H}_k^{\alpha=1}(t)$ can be reduced to $\mu_0 > 0.5\tau$. On the other hand, the trivial-nontrivial transition occurs at $\mu_0 - \frac{\omega}{2} = w_0$, which implies $\mu_0 = \frac{\tau}{2} + \frac{\omega}{4}$. By fixing the frequency, $\omega = 1.5\tau$, we predict TQPTs at zeros

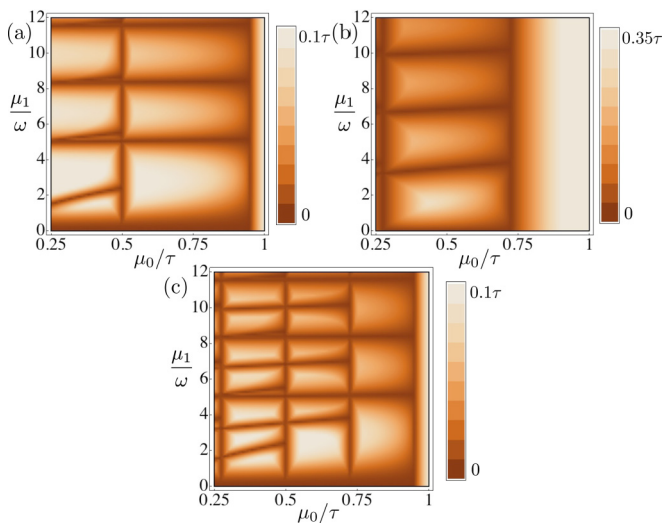


FIG. 7. (Color online) Phase diagram for $\omega = 0.9\tau$ in the case of a driven chemical potential. The dark lines show the closings of (a) the 0 gap, (b) the $\frac{\omega}{2}$ gap, and (c) both gaps. The diagram (c) in the right part is the same as the diagram for $\omega = 1.5\tau$ but changing the zeros of \mathcal{J}_0 by zeros of \mathcal{J}_1 and the zeros of \mathcal{J}_1 by zeros of \mathcal{J}_2 ($\tau = 1$).

of the Bessel function $\mathcal{J}_1(\frac{\mu_{\perp}}{\omega})$, which occur at values $\frac{\mu_{\perp}}{\omega} \in \{3.8, 7.0, 10.2, \dots\}$, in the regime $0.5\tau < \mu_0 < 0.875\tau$ shown in Fig. 6(b). For smaller values of μ_0 , we need to use $\tilde{H}_k^{\alpha=0}(t)$ and $\tilde{H}_k^{\alpha=1}(t)$, as we explained in Sec. II, and consequently we predict TQPTs at zeros of $\mathcal{J}_0(\frac{\mu_{\perp}}{\omega})$ and $\mathcal{J}_1(\frac{\mu_{\perp}}{\omega})$ as in Fig. 6(c).

We show also in Fig. 7 the same calculation for $\omega = 0.9\tau$, in order to see that for large values of μ_0 the analytical approach is useful. For $\frac{2}{3}\tau < \omega < \tau$, the Magnus series of $\tilde{H}_k^{\alpha=2}(t)$ converges if $\mu_0 > \frac{\omega}{4} + \frac{\tau}{2}$. For $\omega = 0.9\tau$, this value is $\mu_0 > 0.725\tau$. On the other hand, the trivial-nontrivial transition occurs at $\mu_0 - \omega = w_0$. This means $\mu_0 = \frac{\tau}{2} + \frac{\omega}{2} = 0.95\tau$. Then, for values $0.725\tau < \mu_0 < 0.95\tau$, the phase diagram shows TQPTs at zeros of $\mathcal{J}_2(\frac{\mu_{\perp}}{\omega})$, which appear at values $\frac{\mu_{\perp}}{\omega} \in \{5.1, 8.4, 11.6, \dots\}$, as is shown in Fig. 7(c). For smaller values of μ_0 , we predict TQPTs at zeros of $\mathcal{J}_2(\frac{\mu_{\perp}}{\omega})$ and $\mathcal{J}_1(\frac{\mu_{\perp}}{\omega})$. However, for even smaller values of μ_0 , our analytical approach is not valid anymore and the phase diagram is more complex.

APPENDIX B: NUMERICAL CALCULATION OF TEMPORAL EVOLUTION

In this Appendix, we want to give more details about the numerical calculation of the temporal evolution shown in Fig. 3. Following the seminal paper of Kitaev [8], one can write the Hamiltonian Eq. (1) as a quadratic form in terms of the Majorana operators a_{2j} and a_{2j-1} ,

$$H(t) = \frac{i}{4} \sum_{l,r} a_l M_{lr}(t) a_r, \quad (\text{B1})$$

where $M(t)$ is a time-periodic real antisymmetric matrix. Motivated by a previous work [35], we calculate the Heisenberg equations of motion for the Majorana operators,

$$\frac{da_l(t)}{dt} = i[H(t), a_l(t)] = \sum_{r=1}^{2N} M_{lr}(t) a_r(t). \quad (\text{B2})$$

Following Refs. [8,35], we construct the column vector $\mathbf{A} = (a_1, a_2, \dots, a_{2N})^T$, which allows us to write Eq. (B2) as follows:

$$\frac{d\mathbf{A}(t)}{dt} = M(t)\mathbf{A}(t). \quad (\text{B3})$$

Now we can build the evolution operator such that $\mathcal{U}(t,0)\mathbf{A}(0) = \mathbf{A}(t)$. Invoking Floquet theory [44], we look for Floquet states of the form $\Psi_l(t) = e^{-i\epsilon_l t} \Upsilon_l(t)$ with Floquet modes $\Upsilon_l(t) = \Upsilon_l(t+T)$ satisfying the eigenvalue equation $\mathcal{U}(T,0)\Upsilon_l(0) = e^{-i\epsilon_l T} \Upsilon_l(0)$. Our aim is to obtain the Majorana field operators corresponding to the end state with quasienergies $\epsilon_l = 0, \pm \frac{\omega}{2}$. In so doing, we just need to find the corresponding $\Upsilon_l(t)$ such that $\mathcal{U}(T,0)\Upsilon_l(0) = \Upsilon_l(0)$ for the $\epsilon_l = 0$ gap, and $\mathcal{U}(T,0)\Upsilon_l(0) = e^{\mp i\pi} \Upsilon_l(0)$ for the $\epsilon_l = \pm \frac{\omega}{2}$ gap. These Majorana field operators can be written in terms of complex fermions,

$$\Psi_l(t) = \sum_{r=1}^N [u_{lr}(t) f_r + v_{lr}(t) f_r^\dagger]. \quad (\text{B4})$$

In the main text, for simplicity, we have dropped the index l in the definition of the Majorana mode of Eq. (B4). The coefficients $u_i(t)$ and $v_i(t)$ are shown in Figs. 3(a) and 3(b) for different cases, and they are in agreement with the predicted ones.

Given an initial condition $\Gamma(0) = f_1 = [a_1(0) + ia_2(0)]$, the evolution is known to be $\Gamma(t) = [a_1(t) + ia_2(t)]$, written

in a general form as

$$\Gamma(t) = \sum_{r=1}^N [\tilde{u}_r(t)f_r + \tilde{v}_r(t)f_r^\dagger]. \quad (\text{B5})$$

-
- [1] C. L. Kane and E. J. Mele, *Phys. Rev. Lett.* **95**, 146802 (2005).
 - [2] B. A. Bernevig, T. L. Hughes, and S.-C. Zhang, *Science* **314**, 1757 (2006).
 - [3] L. Fu, C. L. Kane, and E. J. Mele, *Phys. Rev. Lett.* **98**, 106803 (2007).
 - [4] L. Fu and C. L. Kane, *Phys. Rev. B* **76**, 045302 (2007).
 - [5] D. Hsieh *et al.*, *Nature (London)* **452**, 970 (2008).
 - [6] M. König *et al.*, *Science* **318**, 766 (2007).
 - [7] D. J. Thouless, M. Kohmoto, M. P. Nightingale, and M. den Nijs, *Phys. Rev. Lett.* **49**, 405 (1982).
 - [8] A. Y. Kitaev, *Phys. Usp.* **44**, 131 (2001).
 - [9] J. Alicea, *Rep. Prog. Phys.* **75**, 076501 (2012).
 - [10] M. Z. Hasan and C. L. Kane, *Rev. Mod. Phys.* **82**, 3045 (2010).
 - [11] J.-i. Inoue and A. Tanaka, *Phys. Rev. Lett.* **105**, 017401 (2010).
 - [12] T. Kitagawa, E. Berg, M. Rudner, and E. Demler, *Phys. Rev. B* **82**, 235114 (2010).
 - [13] T. Kitagawa, M. S. Rudner, E. Berg, and E. Demler, *Phys. Rev. A* **82**, 033429 (2010).
 - [14] N. H. Lindner, G. Refael, and V. Galitski, *Nat. Phys.* **7**, 490 (2011).
 - [15] M. S. Rudner, N. H. Lindner, E. Berg, and M. Levin, *Phys. Rev. X* **3**, 031005 (2013).
 - [16] A. Gómez-León and G. Platero, *Phys. Rev. Lett.* **110**, 200403 (2013).
 - [17] L. Jiang, T. Kitagawa, J. Alicea, A. R. Akhmerov, D. Pekker, G. Refael, J. I. Cirac, E. Demler, M. D. Lukin, and P. Zoller, *Phys. Rev. Lett.* **106**, 220402 (2011).
 - [18] T. Kitagawa *et al.*, *Nat. Commun.* **3**, 882 (2012).
 - [19] A. Kundu and B. Seradjeh, *Phys. Rev. Lett.* **111**, 136402 (2013).
 - [20] Q.-J. Tong, J.-H. An, J. Gong, H.-G. Luo, and C. H. Oh, *Phys. Rev. B* **87**, 201109 (2013).
 - [21] J. K. Asbóth, *Phys. Rev. B* **86**, 195414 (2012).
 - [22] J. K. Asbóth and H. Obuse, *Phys. Rev. B* **88**, 121406 (2013).
 - [23] J. K. Asbóth, B. Tarasinski, and P. Delplace, *Phys. Rev. B* **90**, 125143 (2014).
 - [24] V. Mourik *et al.*, *Science* **336**, 1003 (2012).
 - [25] L. P. Rokhinson, X. Liu, and J. K. Furdyna, *Nat. Phys.* **8**, 795 (2012).
 - [26] A. Das *et al.*, *Nat. Phys.* **8**, 887 (2012).
 - [27] M. T. Deng *et al.*, *Nano Lett.* **12**, 6414 (2012).
 - [28] Y. Oreg, G. Refael, and F. von Oppen, *Phys. Rev. Lett.* **105**, 177002 (2010).
 - [29] R. M. Lutchyn, J. D. Sau, and S. Das Sarma, *Phys. Rev. Lett.* **105**, 077001 (2010).
 - [30] F. Domínguez, F. Hassler, and G. Platero, *Phys. Rev. B* **86**, 140503 (2012).
 - [31] D. E. Liu, A. Levchenko, and H. U. Baranger, *Phys. Rev. Lett.* **111**, 047002 (2013).
 - [32] P. Wang, Q.-f. Sun, and X. C. Xie, *Phys. Rev. B* **90**, 155407 (2014).
 - [33] C. C. Wu, J. Sun, F. J. Huang, Y. D. Li, and W. M. Liu, *Europhys. Lett.* **104**, 27004 (2013).
 - [34] A. A. Reynoso and D. Frustaglia, *Phys. Rev. B* **87**, 115420 (2013).
 - [35] M. Thakurathi, A. A. Patel, D. Sen, and A. Dutta, *Phys. Rev. B* **88**, 155133 (2013).
 - [36] Y. Niu, S. B. Chung, C.-H. Hsu, I. Mandal, S. Raghu, and S. Chakravarty, *Phys. Rev. B* **85**, 035110 (2012).
 - [37] J. Dziarmaga, *Phys. Rev. Lett.* **95**, 245701 (2005).
 - [38] A. Das, *Phys. Rev. B* **82**, 172402 (2010).
 - [39] V. M. Bastidas, C. Emary, G. Schaller, and T. Brandes, *Phys. Rev. A* **86**, 063627 (2012).
 - [40] A. Russomanno, A. Silva, and G. E. Santoro, *Phys. Rev. Lett.* **109**, 257201 (2012).
 - [41] E. Lieb, T. Schultz, and D. Mattis, *Ann. Phys. (NY)* **16**, 407 (1961).
 - [42] S. Tewari and J. D. Sau, *Phys. Rev. Lett.* **109**, 150408 (2012).
 - [43] W. DeGottardi, M. Thakurathi, S. Vishveshwara, and D. Sen, *Phys. Rev. B* **88**, 165111 (2013).
 - [44] J. H. Shirley, *Phys. Rev.* **138**, B979 (1965).
 - [45] H. Sambe, *Phys. Rev. A* **7**, 2203 (1973).
 - [46] G. Platero and R. Aguado, *Phys. Rep.* **395**, 1 (2004).
 - [47] S. Blanes, F. Casas, J. A. Oteo, and J. Ros, *Phys. Rep.* **470**, 151 (2009).
 - [48] A. López, A. Scholz, Z. Z. Sun, and J. Schliemann, *Europhys. J. B* **86**, 366 (2013).
 - [49] J. D. Sau and S. D. Sarma, *Nat. Commun.* **3**, 964 (2012).
 - [50] I. C. Fulga, A. Haim, A. R. Akhmerov, and Y. Oreg, *New J. Phys.* **15**, 045020 (2013).